THE JOURNAL OF PHYSICAL CHEMISTRY B

Article

pubs.acs.org/JPCB

Spatio−Temporal Characteristics of the Transfer Free Energy of Apomyoglobin into the Molecular Crowding Condition with Trimethylamine *N*-oxide: A Study with Three Types of the Kirkwood−Buff Integral

Isseki Yu,*[,†,§] Kyoko Nakada,[†] and Masataka Nagaoka[‡,§]

[†]Department of Chemistry and Biological Science, College of Science and Engineering, Aoyama Gakuin University, 5-10-1 Fuchinobe, Chuou-ku, Sagamihara, Kanagawa 252-5258, Japan

[‡]Graduate School of Information Science, Nagoya University, Furo-cho, Chikusa-ku, Nagoya 464-8601, Japan

[§]CREST, Japan Science and Technology Agency, Japan

Supporting Information

ABSTRACT: The transfer free energy (TFE) of apomyoglobin (AMb) from pure water into aqueous solution with trimethylamine *N*-oxide (TMAO) was investigated by all-atom molecular dynamics (MD) simulation combined with the Kirkwood−Buff (KB) integral method. The simulated TFE and the preferential interaction parameter correlated favorably with experimental values. In addition, the time-resolved KB integral revealed that a significant fluctuation in the TFE arose from the alteration in TMAO solvation around AMb. Furthermore, spatial decomposition of the KB integrals revealed how the local elements of the TFE are spatially distributed around AMb. These results revealed the spatio−temporal characteristics of the protein TFE into the molecular crowding condition with TMAO.

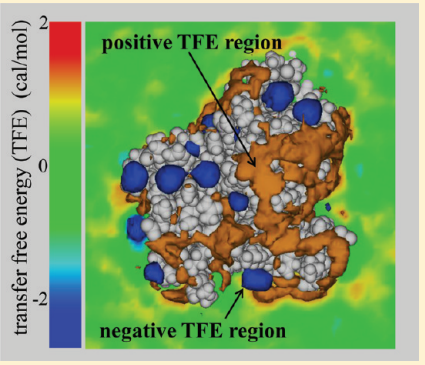

1. INTRODUCTION

The cell contains high concentrations of proteins, nucleic acids, polysaccharides, and low molecular weight compounds in aqueous solution in the cytoplasm. The total concentration of these biomolecules reaches 50−400 g/L,[1−4] and they therefore occupy a significant volume of the cytoplasm. Such molecular crowding conditions arise not only from the presence of the biomacromolecules but also from high concentrations of osmolytes, such as glycerol, sugars, methylamines, ectoines, and amino acids.[5−7] Previous studies have indicated that osmolytes in aqueous solution significantly alter the thermodynamic and kinetic properties of not only proteins and nucleic acids, but also of water molecules.[5−15] However, the molecular mechanisms by which osmolytes act at the microscopic level are not fully understood yet.

The transfer free energy (TFE) of a protein (i.e., the change in Gibbs energy when the protein transfers from the solvent phase into a different phase) is one of the most important thermodynamic quantities that describes the influence of the solution environment. In this study, the TFE of apomyoglobin (AMb) from pure water into an aqueous solution of osmolytes was investigated by all-atom molecular dynamics (MD) simulation. Trimethylamine *N*-oxide (TMAO),[5] which is one of the most common osmolytes found in high concentration in deep-sea fishes, was used to mimic the osmolyte-induced crowding condition.

The spatial and radial distribution functions of water and TMAO molecules were obtained from the MD simulation, and were used to calculate the TFE by the Kirkwood−Buff (KB) integral method.[16−18] Our theoretical TFE value and the preferential interaction parameter showed good correspondence with experimental values. Furthermore, the microscopic characteristics of the TFE were revealed by the space-time deconvolution techniques for KB integrals that we previously developed.[15,19−21] The results provided us with a three-dimensional image and the molecular dynamics characteristics of the protein TFE into the molecular crowding condition with TMAO.

This article is organized as follows: Initially, the computational methods and the model systems are explained. Precise numerical results are provided and discussed in the Results and Discussion sections. Finally, the findings are summarized in the Concluding Remarks section. Detailed numerical techniques are explained in the Appendix.

Received: January 12, 2012
Revised: February 24, 2012
Published: February 29, 2012

2. COMPUTATIONAL METHODS

2.1. Radial Kirkwood−Buff Integral. The Kirkwood−Buff (KB) integral[16−18] of a solvent component s around a certain solute molecule α is defined as

$$G_{\alpha s} = \int_V \{g_{ks}(\mathbf{r}) - 1\}\mathrm{d}\mathbf{r} \tag{1}$$

where $g_{ks}(\mathbf{r})$ is the pair correlation function between one of the atomic sites k of the solute molecule α and the solvent component s at position $\mathbf{r}$. The value of $g_{ks}(\mathbf{r})$ is normalized to 1 for bulk solvent. $\int_V()\mathrm{d}\mathbf{r}$ represents the integral taken in the whole three-dimensional space. The KB integrals, $G_{\alpha s}$, connect the microscopic correlation functions, $g_{ks}(\mathbf{r})$, to the thermodynamic quantities, such as TFE (see section 2.2). With the radial distribution function between k and s, $G_{\alpha s}$ is obtained as follows:

$$G_{\alpha s} = \lim_{R\to\infty} G_{\alpha s}(R) = \lim_{R\to\infty} \int_{r=0}^{r=R} 4\pi r^2\{g_{ks}(r) - 1\}\mathrm{d}r \tag{2}$$

Using the MD-derived solvent configurations at time t, and the number density of s in the bulk solvent phase ρ_s, $G_{\alpha s}$ is given as

$$\begin{aligned} G_{\alpha s} &= \lim_{R\to\infty} G_{\alpha s}(R) \\ &= \lim_{R\to\infty} \langle G_{\alpha s}(R, t)\rangle_T \\ &= \lim_{R\to\infty} \left(\frac{\langle N_{ks}^{\phi}(R, t)\rangle_T}{\rho_s} - (4\pi R^3/3) \right) \end{aligned} \tag{3}$$

where $N_{ks}^{\phi}(R,t)$ is the instantaneous coordination number of s at time t inside the sphere $\phi_k(R,t)$ with the radius R centering on the given atomic site k (Figure 1a). The brackets $\langle ...\rangle_T$ denote the time-average, defined as $1/T\int_0^T(...)\mathrm{d}t$. We refer to the R-dependent KB integral obtained by eqs 2 or 3 as the *radial* KB integral $G_{\alpha s}^{\mathrm{R}}(R)$.

2.2. Surficial Kirkwood−Buff Integral. Although $G_{\alpha s}^{\mathrm{R}}(R)$ is easy to calculate numerically, it is inconvenient for analyzing the profile of $G_{\alpha s}$ because the integration variable R does not directly reflect the shape information of the target solute α. To overcome this problem, we have introduced a solute-shape-dependent KB integral, the *surficial* KB integral $G_{\alpha s}^{\mathrm{S}}(R^{\upsilon})$,[19−21] as

$$\begin{aligned} G_{\alpha s}^{\mathrm{S}} &= \lim_{R^{\upsilon}\to\infty} G_{\alpha s}^{\mathrm{S}}(R^{\upsilon}) \\ &= \lim_{R^{\upsilon}\to\infty} \langle G_{\alpha s}^{\mathrm{S}}(R^{\upsilon}, t)\rangle_T \\ &= \lim_{R^{\upsilon}\to\infty} \left\langle \frac{N_{\alpha s}^{\upsilon}(R^{\upsilon}, t)}{\rho_s} - V_{\upsilon} \right\rangle_T \end{aligned} \tag{4}$$

where $N_{\alpha s}^{\upsilon}(R^{\upsilon},t)$ is the instantaneous coordination number of s inside the hypothetical spatial region $\upsilon_{\alpha}(R^{\upsilon},t)$ surrounding the solute molecule α at time t. V_{υ} is the volume of the region $\upsilon_{\alpha}(R^{\upsilon},t)$. The boundary of $\upsilon_{\alpha}(R^{\upsilon},t)$ is defined as the surface whose distance to the nearest atomic center of α is R^{υ} (Figure 1b). The details of the definitions are shown in our previous work.[19]

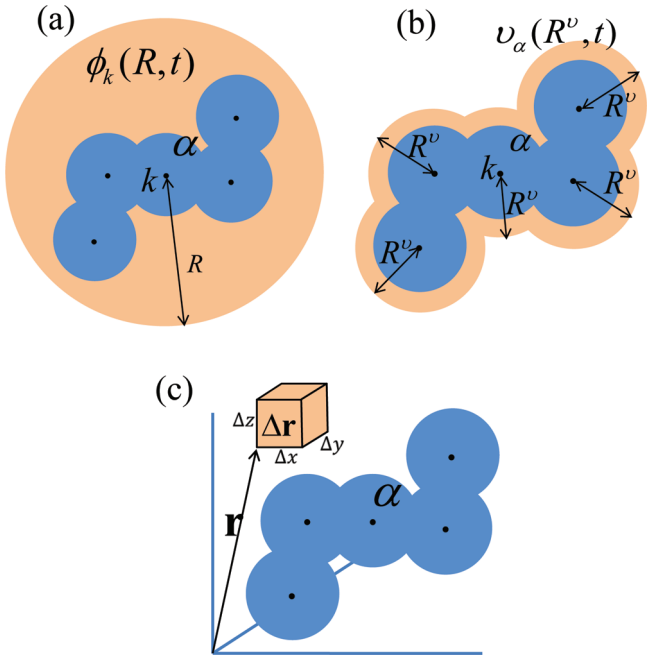

Figure 1. Schematic explanations of the three types of KB integral around the solute molecule α (blue filled circles). The upper limits of the integration ranges are represented as the *outer boundary* of the orange regions. (a) Radial KB integral $G_{\alpha s}^{\mathrm{R}}(R)$: the integration range is defined as the sphere with the radius R centering on the arbitrary atomic site k. (b) Surficial KB integral $G_{\alpha s}^{\mathrm{S}}(R^{\upsilon})$: the integration range is the instantaneous hypothetical spatial region $\upsilon_{\alpha}(R^{\upsilon},t)$ surrounding α. The boundary of $\upsilon_{\alpha}(R^{\upsilon},t)$ is defined as the surface whose distance to the nearest atomic center of α at time t is R^{υ}. (c) Elemental KB integral $G_{\alpha s}^{\mathrm{E}}(\mathbf{r})$: the integration range is the small region $\Delta\mathbf{r}$ at the position $\mathbf{r}$ (= x, y, z) whose volume is $\Delta x\Delta y\Delta z$.

2.3. Elemental Kirkwood−Buff Integral. The *elemental* KB integral $G_{\alpha s}^{\mathrm{E}}(\mathbf{r})$, which is the local element of the KB integral in the region $\Delta\mathbf{r}$ at position $\mathbf{r}$= (x, y, z), is defined as

$$\begin{aligned} G_{\alpha s}^{\mathrm{E}}(\mathbf{r}) &= \langle G_{\alpha s}^{\mathrm{E}}(\mathbf{r}, t)\rangle_T \\ &= \int_x^{x+\Delta x}\int_y^{y+\Delta y}\int_z^{z+\Delta z} \left\{ \frac{\langle \rho_s(x, y, z, t)\rangle_T}{\rho_s} - 1 \right\} \mathrm{d}x\,\mathrm{d}y\,\mathrm{d}z \end{aligned} \tag{5}$$

where $\rho_s(x,y,z,t)$ is the instantaneous number density of s in an infinitesimal element of the volume $\mathrm{d}x\,\mathrm{d}y\,\mathrm{d}z$ at position $\mathbf{r}$. $G_{\alpha s}^{\mathrm{E}}(\mathbf{r})$ is numerically calculated as

$$G_{\alpha s}^{\mathrm{E}}(\mathbf{r}) = \frac{\langle N_{\alpha s}^{\Delta\mathrm{r}}(\mathbf{r}, t)\rangle_T}{\rho_s} - \Delta x\Delta y\Delta z \tag{6}$$

where $N_{\alpha s}^{\Delta\mathrm{r}}(\mathbf{r},t)$ is the instantaneous coordination number of s inside the region $\Delta\mathbf{r}$ at position $\mathbf{r}$ whose volume is $\Delta x\Delta y\Delta z$ (Figure 1c).

The radial KB integral $G_{\alpha s}^{\mathrm{R}}(R)$, the surficial KB integral $G_{\alpha s}^{\mathrm{S}}(R^{\upsilon})$, and the elemental KB integral $G_{\alpha s}^{\mathrm{E}}(\mathbf{r})$ give exactly the

dx.doi.org/10.1021/jp300380p | J. Phys. Chem. B 2012, 116, 4080−4088

same constant value when their integrations reach the bulk solvent phase

$$G_{\alpha s} = \lim_{R\to\infty} G^{\mathrm{R}}_{\alpha s}(R) = \lim_{R^{\upsilon}\to\infty} G^{\mathrm{S}}_{\alpha s}(R^{\upsilon}) = \int_V G^{E}_{\alpha s}(\mathbf{r})\mathrm{d}\mathbf{r} \tag{7}$$

$G^{\mathrm{R}}_{\alpha s}(R)$ is quick to calculate and is convenient for obtaining the time average value of the related thermodynamic quantities from the large number of MD-derived snapshots. The larger integration range can be used in this type of KB integral. Calculation of $G^{\mathrm{S}}_{\alpha s}(R^{\upsilon})$ is much more time-consuming; however, it provides us with a clearer understanding of the profile of the KB integral and the related thermodynamic quantities *as functions of the distance from the solute surface*. The final integral $G^{\mathrm{E}}_{\alpha s}(\mathbf{r})$ is convenient for determining the three-dimensional distributions of the thermodynamic quantities around the target solute.

2.4. Transfer Free Energy of Apomyoglobin from Pure Water into Aqueous Solution with TMAO. In this section, we derive equations for a system with the three components, water, TMAO, and AMb, where AMb is very dilute ($\rho_{\mathrm{a}} \to 0$) in the mixture of water and TMAO. In the present study, subscripts a, w, and t indicate AMb, water, and TMAO, respectively. Unfortunately, both Gibbs energy and the KB integral have been denoted by the same symbol "G". In the present study, we use $\mathcal{G}$ for Gibbs energy to distinguish it from KB integral G.

The slope of the solvation Gibbs energy of AMb $\Delta\mathcal{G}^{*}_{\mathrm{a}}$ as a function of the number density of TMAO ρ_{t} is obtained as[17,18]

$$\lim_{\rho_{\mathrm{a}}\to 0}\left(\frac{\partial\Delta\mathcal{G}^{*}_{\mathrm{a}}}{\partial\rho_{\mathrm{t}}}\right)_{P,T} = kT\frac{2V_{\mathrm{w}}(\rho_{\mathrm{t}}+\rho_{\mathrm{w}})-1}{\rho_{\mathrm{t}}(G_{\mathrm{tw}}-G_{\mathrm{tt}})-1}(G_{\mathrm{at}}-G_{\mathrm{aw}}) \tag{8}$$

where k and T are Boltzmann constant and temperature, respectively (the derivation of eq 8 is partially explained in Appendix A). ρ_{w} is the number density of water molecules. G_{tw} and G_{tt} are the KB integrals between solvent molecules in the bulk solvent phase. G_{at} and G_{aw} are the KB integral of TMAO and that of water around AMb, respectively. V_{w} is the partial molar volume of a water molecule obtained by[17,18]

$$V_{\mathrm{w}} = \frac{1+\rho_{\mathrm{t}}(G_{\mathrm{tt}}-G_{\mathrm{tw}})}{\rho_{\mathrm{w}}+\rho_{\mathrm{t}}+\rho_{\mathrm{w}}\rho_{\mathrm{t}}(G_{\mathrm{ww}}+G_{\mathrm{tt}}-2G_{\mathrm{tw}})} \tag{9}$$

It is experimentally understood that the solvation Gibbs energy of proteins is a linear function of osmolyte concentration.[9−13,22,33] Using this tenet, the TFE of AMb ($\Delta\mathcal{G}^{\mathrm{tr}}_{\mathrm{a}}$) from pure water into the aqueous solution of TMAO with a number density ρ_{t} is estimated as

$$\begin{aligned}\Delta\mathcal{G}^{\mathrm{tr}}_{\mathrm{a}} &= \int_0^{\rho_{\mathrm{t}}}\lim_{\rho_{\mathrm{a}}\to 0}\left(\frac{\partial\Delta\mathcal{G}^{*}_{\mathrm{a}}}{\partial\rho_{\mathrm{t}}}\right)_{P,T}\mathrm{d}\rho_{\mathrm{t}}\\ &= kT\frac{2V_{\mathrm{w}}(\rho_{\mathrm{t}}+\rho_{\mathrm{w}})-1}{\rho_{\mathrm{t}}(G_{\mathrm{tw}}-G_{\mathrm{tt}})-1}\rho_{\mathrm{t}}(G_{\mathrm{at}}-G_{\mathrm{aw}})\end{aligned} \tag{10}$$

For convenience, we define the auxiliary quantities as

$$\xi = \frac{2V_{\mathrm{w}}(\rho_{\mathrm{t}}+\rho_{\mathrm{w}})-1}{\rho_{\mathrm{t}}(G_{\mathrm{tw}}-G_{\mathrm{tt}})-1} \tag{11}$$

Using the radial KB integrals (eqs 2 and 3), $\Delta\mathcal{G}^{\mathrm{tr}}_{\mathrm{a}}$, is given by

$$\Delta\mathcal{G}^{\mathrm{tr}}_{\mathrm{a}} = \lim_{R\to\infty} kT\xi\rho_{\mathrm{t}}\langle G^{\mathrm{R}}_{\mathrm{at}}(R,t) - G^{\mathrm{R}}_{\mathrm{aw}}(R,t)\rangle_T \tag{12}$$

With the surficial KB integrals (eq 4), the R^{υ}-dependent profile of TFE, $\Delta\mathcal{G}^{\mathrm{tr}}_{\mathrm{a}}(R^{\upsilon})$, is given by

$$\begin{aligned}\Delta\mathcal{G}^{\mathrm{tr}}_{\mathrm{a}}(R^{\upsilon}) &= \langle\Delta\mathcal{G}^{\mathrm{tr}}_{\mathrm{a}}(R^{\upsilon},t)\rangle_T\\ &= kT\xi\rho_{\mathrm{t}}\langle G^{\mathrm{S}}_{\mathrm{at}}(R^{\upsilon},t) - G^{\mathrm{S}}_{\mathrm{aw}}(R^{\upsilon},t)\rangle_T\end{aligned} \tag{13}$$

Finally, the three-dimensional distribution of the TFE $\Delta\mathcal{G}^{\mathrm{tr}}_{\mathrm{a}}(\mathbf{r})$ is obtained from the elemental KB integral (eqs 5 and 6) as

$$\begin{aligned}\Delta\mathcal{G}^{\mathrm{tr}}_{\mathrm{a}}(\mathbf{r}) &= \langle\Delta\mathcal{G}^{\mathrm{tr}}_{\mathrm{a}}(\mathbf{r},t)\rangle_T\\ &= kT\xi\rho_{\mathrm{t}}\langle G^{\mathrm{E}}_{\mathrm{at}}(\mathbf{r},t) - G^{\mathrm{E}}_{\mathrm{aw}}(\mathbf{r},t)\rangle_T\end{aligned} \tag{14}$$

$\Delta\mathcal{G}^{\mathrm{tr}}_{\mathrm{a}}(R^{\upsilon})$ and $\Delta\mathcal{G}^{\mathrm{tr}}_{\mathrm{a}}(\mathbf{r})$ give exactly the same TFE value calculated by eq 12 when their integrations reach the bulk solvent phase

$$\Delta\mathcal{G}^{\mathrm{tr}}_{\mathrm{a}} = \lim_{R^{\upsilon}\to\infty}\Delta\mathcal{G}^{\mathrm{tr}}_{\mathrm{a}}(R^{\upsilon}) = \int_V \Delta\mathcal{G}^{\mathrm{tr}}_{\mathrm{a}}(\mathbf{r})\mathrm{d}\mathbf{r} \tag{15}$$

$\Delta\mathcal{G}^{\mathrm{tr}}_{\mathrm{a}}(R^{\upsilon})$, however, provides us with a clearer understanding of the profile of the TFE *as a function of the distance from the solute surface*. The final integral $\Delta\mathcal{G}^{\mathrm{tr}}_{\mathrm{a}}(\mathbf{r})$ is convenient for determining the three-dimensional distribution of TFE.

2.5. Molecular Dynamics Simulations. MD calculations were performed using the AMBER10 program.[23] The force field parameter set ff03[24] was used for AMb. As for the TMAO molecules, parameters[25] previously developed based on the AMBER type force field were adopted. The crystal structure of sperm whale myoglobin was retrieved from the PDB entry, 104M. The initial atomic coordinates for the AMb were taken from those of the crystal structure with the heme group removed. The molecular crowding condition with TMAO was reproduced with a mixture of 2598 TMAO molecules and 56315 TIP4P water molecules.[26] The concentration of TMAO was about 170 g/L (2.19 M), which corresponds to the typical intracellular crowding condition. After the system was initially equilibrated for 5 ns at a pressure of 1 bar and a temperature of 298 K, a 25 ns production MD run was executed at the same temperature and the same pressure. We refer to this system and its MD simulation as MDp.

To investigate the solvation properties of water and TMAO molecules in the bulk solvent phase, another MD simulation of the TMAO aqueous solution was independently executed (we refer to this system and its MD simulation as MDb). In MDb, the total numbers of TMAO and water molecules were the same as those in MDp, but the solute protein AMb was eliminated. After equilibration, a 5 ns production MD run was performed at the same pressure and temperature as in MDp.

All the MD simulations were performed under the NPT condition, using the Berendsen algorithm[27] for temperature and pressure regulation. Trajectories were numerically integrated by the velocity Verlet method with a time step of 2.0 fs. The electrostatic interactions were treated by the particle-mesh Ewald (PME) method.[28] Bonds involving hydrogen atoms were constrained by the SHAKE method.[29] The final system size was about 125 × 125 × 125 Å^3, containing 253 689 atoms. The system size was large enough to analyze the solvent structure

dx.doi.org/10.1021/jp300380p | J. Phys. Chem. B 2012, 116, 4080−4088

around the AMb. One of the snapshots of the system is shown in Figure 2.

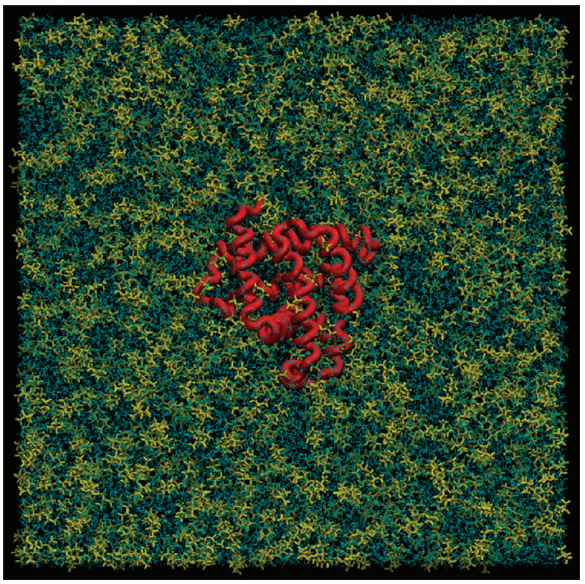

Figure 2. Snapshot of the AMb (red tube) in the periodic boundary box filled with 56 315 water molecules (ice blue lines) and 2598 TMAO molecules (yellow sticks). The picture shows the cross sectional surface near the AMb. The final system size is about 125 × 125 × 125 Å.

3. RESULTS AND DISCUSSION

3.1. Kirkwood Buff Integrals between Water and TMAO Molecules. To estimate the TFE of AMb from eqs 10 and 12−14, KB integrals between solvent components in the bulk solvent phase (G_{tw}, G_{ww}, and G_{tt}) were required. Based on eq 2, those values were calculated using the radial distribution functions (RDFs) between the oxygen atoms in TMAO and water molecules. Atomic configurations generated by the simulation MDb were used for the calculation. The upper limit of the integration range was substituted with R = 20.0 Å, which is a large enough radius for RDFs to converge, instead of infinite distance ∞ in eq 2. Results are shown in Table 1 with number density of TMAO and water molecules (ρ_w and ρ_t).

To understand how the KB integral of water fluctuates around TMAO, the R-dependent increment of the KB integral defined as

$$\delta G^{R}_{tw}(R) = G^{R}_{tw}(R + \Delta r) - G^{R}_{tw}(R) \tag{16}$$

was analyzed (Figure 3a). The step size Δr was set to 0.1 Å. In the same manner, the profiles between TMAO molecules $\delta G^{R}_{tt}(R)$ (Figures 3b) and between water molecules $\delta G^{R}_{ww}(R)$ (Figures 3c) were also analyzed. $\delta G^{R}_{tw}(R)$ showed a sharp positive peak at R = 2.8 Å (Figure 3a), while $\delta G^{R}_{tt}(R)$ exhibited broad negative peaks until $R \approx$ 5.0 Å (Figure 3b). These results indicate that TMAO molecules strongly attract water molecules but do not significantly attract each other. Observation of the sharp first peak in $\delta G^{R}_{tw}(R)$ (Figure 3a) indicates that water molecules form a distinct hydration shell around the oxygen atoms in each TMAO. In addition, previous work indicated that the presence of the nitrogen atom partially neutralizes the hydrophobic effects of the methyl groups in TMAO.[25] These effects should prevent the self-aggregation of TMAO molecules, even at high concentrations.

3.2. Transfer Free Energy of Apomyoglobin into the Molecular Crowding Condition with TMAO. To calculate the time-average of TFE by eq 12, we used the radial KB integrals. The upper limit of the integration range in eq 3 was replaced by R = 50.0 Å instead of the infinite distance, $R = \infty$. 2500 snapshots extracted uniformly from the entire time duration of the MDp were used for the calculation (the numerical procedure explained in Appendix B). Preferential interaction parameter Γ[9−11,15,30] defined as

$$\begin{aligned}\Gamma &= N^{ex}_{at} - \frac{\rho_t}{\rho_w} N^{ex}_{aw} \\ &= \rho_t (G_{at} - G_{aw}) \\ &= \lim_{R\to\infty} \rho_t \langle G^{R}_{at}(R, t) - G^{R}_{aw}(R, t)\rangle_T \end{aligned} \tag{17}$$

was also calculated. In eq 17, N^{ex}_{at} and N^{ex}_{aw} indicate the excess coordination number of TMAO and water molecules around AMb, respectively. Note that by using $\Gamma = \rho_t(G_{at} - G_{aw})$, TFE defined by eq 10 can be simply defined as

$$\Delta \mathcal{G}^{tr}_{a} = kT\xi\Gamma \tag{18}$$

In the case of our system, the sign of the $kT\xi$ is negative. Therefore, the value of TFE is proportional to −Γ. In other words, a negative (positive) value in Γ means that TMAO molecules are preferentially excluded (associated) from (to) AMb, thus making the TFE positive (negative).

We obtained Γ = −12.2 (mol/mol) and $\Delta \mathcal{G}^{tr}_{a}$ = 10.1 (kcal/mol). These values compared favorably with experimental or theoretical values obtained in various crowding conditions with osmolytes[8−11,31−33] (Table 2). Furthermore, Bolen and co-workers estimated the TFE of amino acids from pure water into an aqueous solution of 1.0 M TMAO.[31] Using their data, we estimated that the average TFE of amino acids (into 1.0 M TMAO) was 0.157 (kcal/mol). Then, we estimated the TFE of AMb into the solvent condition of our system by linear extrapolation using the solvent accessible surface areas (SASAs) and the TMAO concentration as

$$\Delta \mathcal{G}^{tr}_{a} = 0.157 \times N^{res}_{a} \times \frac{S_a}{\overline{S}_p N^{res}_{a}} \times \frac{C_t}{1} \tag{19}$$

where N^{res}_{a} (153) and S_a (7600 Å^2) are the peptide length and the SASA of the AMb (substituted with that of myoglobin),[34] respectively. $\overline{S}_p$ (175.4 Å^2) is the average SASA of amino

Table 1. Number Densities of Water and TMAO Molecules in the Bulk Solvent Phase (ρ_w, ρ_t) and KB Integrals between Solvent Component Pairs (G_{ww}, G_{wt}, G_{tw}, G_{tt})[a]

ρ_w (10^{-2} Å^{-3})	ρ_t (10^{-2} Å^{-3})	G_{ww} (Å^3)	G_{wt} (Å^3)	G_{tw} (Å^3)	G_{tt} (Å^3)
2.720	0.133	−22.69	−65.62	−65.62	−417.64

[a]The upper limit of the integration range was set to R = 20.0 Å.

dx.doi.org/10.1021/jp300380p | J. Phys. Chem. B 2012, 116, 4080−4088

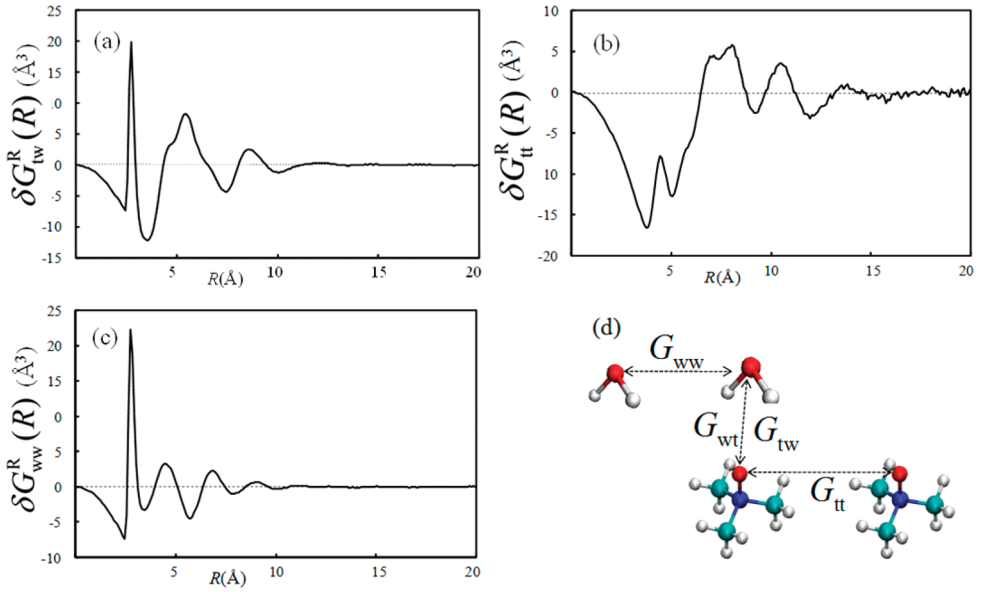

Figure 3. Profiles of the increment of KB integrals between (a) TMAO and water $\delta G^{R}_{tw}(R)$ ($\delta G^{R}_{wt}(R)$), (b) TMAO and TMAO $\delta G^{R}_{tt}(R)$, and (c) water and water $\delta G^{R}_{ww}(R)$. The step size Δr in eq 16 was set to 0.1 Å. A schematic representation of the relationship of molecules considered in KB integrals is shown in d.

Table 2. KB Integrals (G_{aw} and G_{at}), the Preferential Interaction Parameter Γ, and the TFE of AMb into the Crowding Condition with 2.19 M TMAO ($\Delta\mathcal{G}^{tr}_{a}$) (Calcd Line)[a]

		G_{aw} (Å^3)	G_{at} (Å^3)	Γ (mol/mol)	$\Delta\mathcal{G}^{tr}_{a}$ (kcal/mol)
calcd		−20105	−29280	−12.2	10.1
exp	[a1]			−19.9	12
	[a2]			−23.8	4.1
	[a3]			−11.3	3.6
	[a4]			7.6	4.1
	[b]			−11.9	
	[c]				0.157
	[d]				0.087
	[e]				0.329

[a]The upper limit of the integration range was set to R = 50.0 Å. 2500 snapshots extracted uniformly from the entire time durations of the simulation MDp were used for the calculations. Related experimental values are also shown in the exp. line. [a1]Experimental Γ and $\Delta\mathcal{G}^{tr}_{\alpha}$ of bovine serum albumin in 20% sorbitol (refs 8 and 9). [a2]Experimental Γ and $\Delta\mathcal{G}^{tr}_{\alpha}$ of lysozyme in 2 M glycine, (ref 8). [a3]Experimental Γ and $\Delta\mathcal{G}^{tr}_{\alpha}$ of lysozyme in 30% glycerol (ref 8). [a4]Experimental Γ and $\Delta\mathcal{G}^{tr}_{\alpha}$ of ribonuclease A in 1 M sucrose (refs 8 and 10). [b]Experimental Γ for ribonuclease A in 30% glycerol (ref 11). [c]Average TFE of amino acids from water into 1.0 M TMAO aqueous solution (ref 31). [d]Experimental $\Delta\mathcal{G}^{tr}_{\alpha}$ per mol of peptide backbone unit in 1.0 M TMAO aqueous solution (ref 32). [e]Theoretical $\Delta\mathcal{G}^{tr}_{\alpha}$ per mol of peptide backbone unit in 2.0 M TMAO aqueous solution (ref 33).

acids.[34] C_t (=2.19 M) is the concentration of TMAO in the present system. The $\Delta\mathcal{G}^{tr}_{a}$ estimated by eq 19 was 14.9 (kcal/mol), which is also comparable to our theoretical $\Delta\mathcal{G}^{tr}_{a}$ derived from the KB integrals (10.1 (kcal/mol)).

According to eq 10, the value of the TFE is partially determined by the KB integrals between the solvent components G_{tt} and G_{tw}, and this indicates that interaction between TMAO and water molecules is one of the important factors determining TFE. It is therefore suggested that, if each TMAO molecule accumulates water molecules more strongly, the access of TMAO molecules to the protein surface would be more difficult. Such a change in the TMAO-water interaction should reduce the Γ and increase the TFE. Modification of the atomic charge distribution in TMAO may help to refine those thermodynamic quantities.

3.3. R^{υ}-Dependent Profile of the Transfer Free Energy.

To elucidate how the distribution of water and TMAO molecules around AMb contribute to the TFE, the surficial KB integrals $G^{S}_{aw}(R^{\upsilon})$ and $G^{S}_{at}(R^{\upsilon})$ were analyzed. The upper limit of the integration range was set to R^{υ} = 25.0 Å. Figure 4a shows the profiles of the $G^{S}_{as}(R^{\upsilon})$ increment defined as

$$\delta G^{S}_{as}(R^{\upsilon}) = G^{S}_{as}(R^{\upsilon} + \Delta r) - G^{S}_{as}(R^{\upsilon}) \quad (20)$$

The step size Δr was set to 0.1 Å. The profile of water, $\delta G^{s}_{aw}(R^{\upsilon})$, exhibited a deep minimum from $R^{\upsilon} \approx 0.0$ to 2.5 Å. This arises from the steric exclusion of water molecules from the van der Waals spheres of the constituent atoms of AMb. A sharp positive peak in $\delta G^{s}_{aw}(R^{\upsilon})$ from $R^{\upsilon} \approx 2.5$ to 4.0 Å has an origin in the strong association of water molecules that form the first hydration layer surrounding AMb. In contrast, the profile of TMAO, $\delta G^{s}_{at}(R^{\upsilon})$, showed a more broad minimum from $R^{\upsilon} \approx 0.0$ to 4.0 Å, implying that the TMAO molecules are more strongly excluded from the vicinity of the AMb. No significant fluctuation in $\delta G^{s}_{at}(R^{\upsilon})$ was observed after the very slight increment from $R^{\upsilon} \approx 4.0$ to 6.0 Å. The results indicate that there were no specific interactions between TMAO and AMb from the *time-average viewpoint* in our MD simulation.

Using $\delta G^{s}_{aw}(R^{\upsilon})$, $\delta G^{s}_{at}(R^{\upsilon})$ and eq 13, we obtained the R^{υ}-dependent profile of the TFE $\Delta\mathcal{G}^{tr}_{a}(R^{\upsilon})$. Figure 4b shows the profile of the $\Delta\mathcal{G}^{tr}_{a}(R^{\upsilon})$ increment defined by

$$\delta\Delta\mathcal{G}^{tr}_{a}(R^{\upsilon}) = \Delta\mathcal{G}^{tr}_{a}(R^{\upsilon} + \Delta r) - \Delta\mathcal{G}^{tr}_{a}(R^{\upsilon}) \quad (21)$$

According to the definition of TFE in eq 13, the profile $\delta\Delta\mathcal{G}^{tr}_{a}(R^{\upsilon})$ becomes similar to the subtraction of the two profiles (i.e., subtraction of the blue profile from the red one) in

dx.doi.org/10.1021/jp300380p | J. Phys. Chem. B 2012, 116, 4080−4088

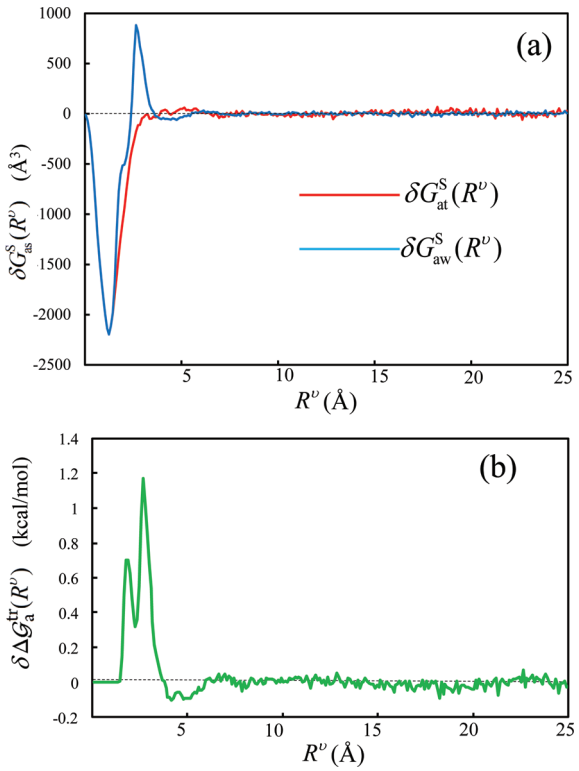

Figure 4. (a) R^υ-dependent profiles of the $G^S_{as}(R^\upsilon)$ increment for water $\delta G^S_{aw}(R^\upsilon)$ (blue) and that for TMAO $\delta G^S_{at}(R^\upsilon)$ (red) around AMb. (b) The R^υ-dependent profile of the TFE increment $\delta\Delta\mathcal{G}^{tr}_a(R^\upsilon)$. The upper limit of the integration range was set to R^υ = 25.0 Å. To obtain their numerical values, Δr (in eqs 20 and 21) was set to 0.1 Å. Two hundred fifty snapshots extracted uniformly from the entire time duration of the simulation (MDp) were utilized for the analysis.

Figure 4a. In the profile of Figure 4b, two positive peaks in the vicinity of AMb are recognized. The first positive peak, from $R^\upsilon \approx$ 1.5 to 2.3 Å, mainly comes from the stronger steric exclusion of TMAO from the AMb surface. The strongest positive peak emerges at around R^υ=3.0 Å, where water molecules form the first hydration layer. Because the formation of the hydration layer reinforces the preferential exclusion of TMAO, $\delta\Delta\mathcal{G}^{tr}_a(R^\upsilon)$ increases more strongly in this region. The slight minimum in $\delta\Delta\mathcal{G}^{tr}_a(R^\upsilon)$ is found from $R^\upsilon \approx$ 4.0 to 6.0 Å, which arises from the first minimum of the density fluctuation of water molecules. The fluctuation of TFE converges to zero about 10 Å from the AMb surface.

3.4. Time Dependency of the Transfer Free Energy and its Influence on the Protein Structure. The total amount of TFE $\Delta\mathcal{G}^{tr}_a$ (section 3.2) and its R^υ-dependence $\Delta\mathcal{G}^{tr}_a(R^\upsilon)$ (section 3.3) indicate that TMAO molecules were preferentially excluded from the vicinity of the AMb surface, and the TFE of AMb into aqueous solution with 2.19 M TMAO exhibited a positive value (10.1 kcal/mol). However, this is the time-average picture (at the 25-ns-time resolution) of the influence of TMAO addition. In this section, we discuss the time-dependency of the TFE.

We again used the surficial KB integrals, and calculated the time-resolved TFE $\Delta\mathcal{G}^{tr}_a(R^\upsilon, t)$ by eq 13. We set the upper limit of the integration range R^υ=10.0 Å, within which the profile of $\delta\Delta\mathcal{G}^{tr}_a(R^\upsilon)$ converges to zero (see Figure 4b).

At first, the trajectory of the time-resolved surficial KB integrals for water $G^S_{aw}(R^\upsilon, t)$ and TMAO $G^S_{at}(R^\upsilon, t)$ were analyzed (Figure 5a.) It was found that $G^S_{aw}(R^\upsilon, t)$ showed an

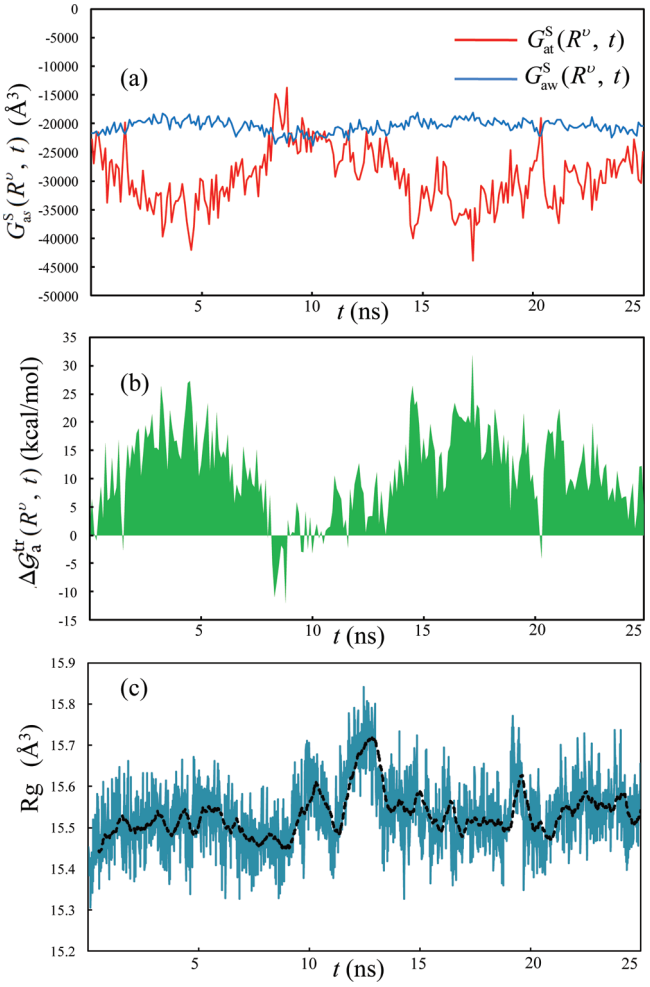

Figure 5. (a) Time histories of the surficial KB integral of water $G^S_{aw}(R^\upsilon, t)$ (blue) and TMAO $G^S_{at}(R^\upsilon, t)$ (red). (b) Time history of TFE $\Delta\mathcal{G}^{tr}_a(R^\upsilon, t)$. The upper limit of the integration range R^υ was set to 10.0 Å. (c) Time history of the radius of gyration Rg of AMb (with a running average of consecutive 50 values: black line).

almost constant trajectory fluctuating around −20000 Å^3. In contrast, the trajectory of TMAO $G^S_{at}(R^\upsilon, t)$ varied from −45000 to −15000 Å^3 and showed a much larger fluctuation than that of water. This indicates that the density fluctuation of TMAO around AMb is more dynamic than that of water. The time duration in which $G^S_{at}(R^\upsilon, t)$ is lower than $G^S_{aw}(R^\upsilon, t)$ (i.e., $\Gamma < 0$) means that the preferential exclusion of TMAO occurs in this period.

Using these two trajectories $G^S_{aw}(R^\upsilon, t)$ and $G^S_{at}(R^\upsilon, t)$, the time history of the TFE $\Delta\mathcal{G}^{tr}_a(R^\upsilon, t)$ was obtained by eq 13 (Figure 5b). As discussed in section 3.2, the value of TFE is proportional to $-\Gamma$ ($= \rho_t(G^s_{aw}(R^\upsilon, t) - G^s_{at}(R^\upsilon, t))$). In addition, the trajectory of water $G^S_{aw}(R^\upsilon, t)$ does not significantly change during the entire time duration. Therefore, the trajectory of TFE $\Delta\mathcal{G}^{tr}_a(R^\upsilon, t)$ exhibited nearly symmetrical fluctuation compared to that of $G^S_{at}(R^\upsilon, t)$ (compare the red trajectory in Figure 5a and the green one in Figure 5b).

dx.doi.org/10.1021/jp300380p | J. Phys. Chem. B 2012, 116, 4080−4088

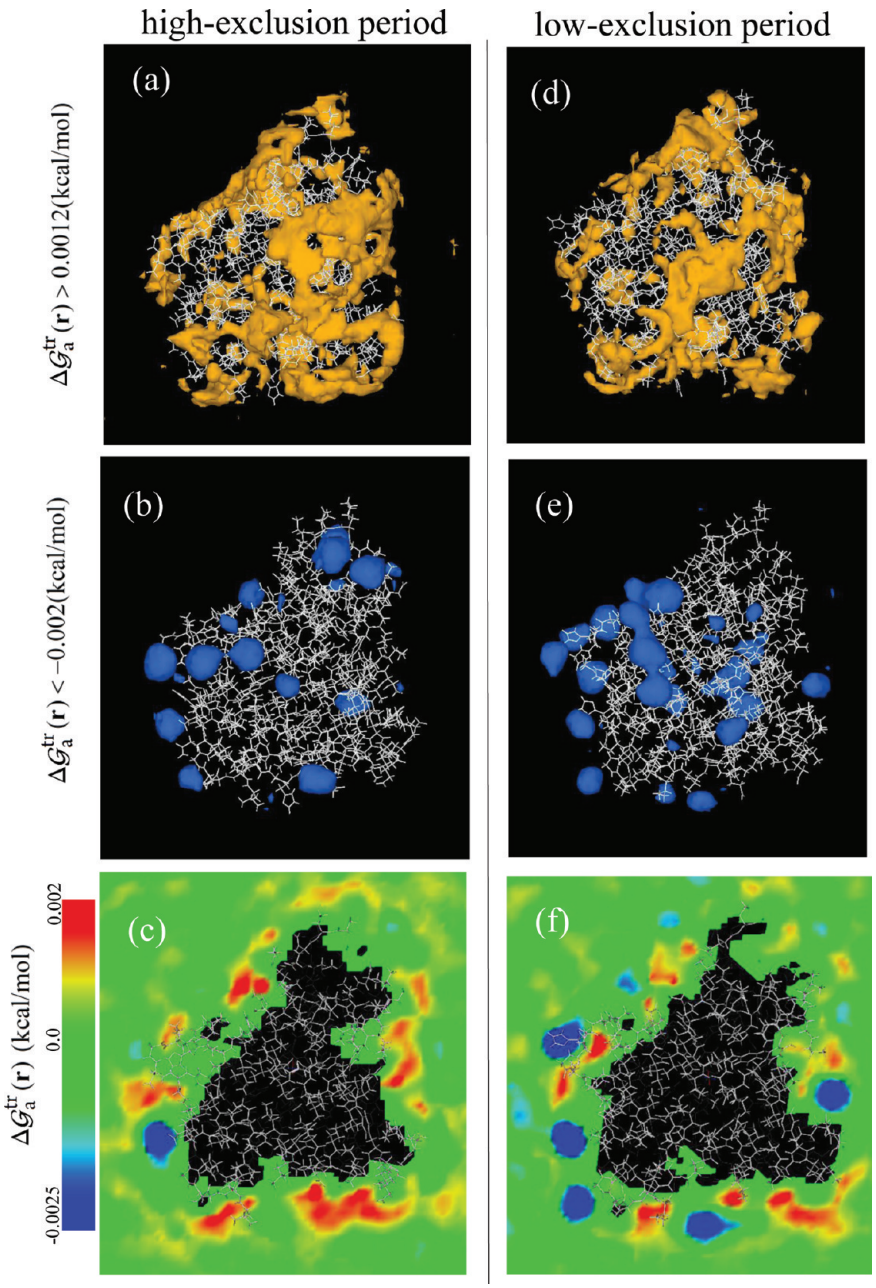

Figure 6. Three-dimensional distributions of the TFE, $\Delta\mathcal{G}_a^{tr}(\mathbf{r})$s, in the high-exclusion period (a–c) and in the low-exclusion period (d–f). (a, d) Positive TFE regions in which the $\Delta\mathcal{G}_a^{tr}(\mathbf{r})$s are more than 0.0012 kcal/mol. (b, e) Negative TFE regions in which $\Delta\mathcal{G}_a^{tr}(\mathbf{r})$s are less than −0.002 kcal/mol. (c, f) The cross sectional view of $\Delta\mathcal{G}_a^{tr}(\mathbf{r})$s. Three thousand snapshots extracted from each period were used for the analysis. The data was analyzed with a resolution of 1.0 Å^3. To obtain clear images *without constraining the protein conformation*, all atomic positions in each snapshot (including solvent atoms) were translated and rotated to minimize the root-mean-square displacement (rmsd) of the protein conformations.

The presence of the preferential exclusion increases the solvation Gibbs energy of the solute protein. Therefore, to reduce the amount of the preferential exclusion, the solute protein prefers a compact conformation like a native one. This is the widely accepted explanation for the stabilizing effect of osmolytes, including TMAO. On the other hand, it is very interesting to find the time periods in which $\Delta\mathcal{G}_a^{tr}(R^{\upsilon}, t)$ have near zero (or even negative) values (e.g., $t \approx 8.0$–14.0 ns). The reduction of the $\Delta\mathcal{G}_a^{tr}(R^{\upsilon}, t)$ comes from the significant increment of $G_{at}^{S}(R^{\upsilon}, t)$. The results imply that although TMAO molecules are preferentially excluded from the protein surface *on average*, they transiently stop to act as stabilizers. Such time durations continued for several nanoseconds.

To investigate the influence of the $\Delta\mathcal{G}_a^{tr}(R^{\upsilon}, t)$ fluctuation on the protein structure, change in the radius of gyration (R_g) of AMb was analyzed. The time history of the R_g exhibited a noticeable increment from $t \approx 10.0$ to 13.0 ns. Such an R_g increment occurred within a time period in which the $\Delta\mathcal{G}_a^{tr}(R^{\upsilon}, t)$ exhibited relatively small values. These data suggest the possibility that the transient weakening of preferential exclusion of TMAO makes the conformation of AMb less compact. However, a much longer MD simulation is needed to

dx.doi.org/10.1021/jp300380p | *J. Phys. Chem. B* 2012, 116, 4080–4088

elucidate the correspondence between the fluctuation of TFE and the structural change of AMb.

3.5. Three-Dimensional Distribution of the Local Elements of Transfer Free Energy. The R^{ν}-dependent profile of TFE (Figure 4b) indicated that most of the increase and decrease in TFE occurred within about 10 Å from the AMb surface. In order to understand the spatial distribution of the TFE at the microscopic level, local elements of the TFE, $\Delta\mathcal{G}_a^{tr}(\mathbf{r})$ values, were analyzed. On the basis of the time history of TFE (see Figure 5b), the time durations t = 2−5 ns and t = 8−11 ns were selected for analysis in this section. These time durations are referred to as *high-exclusion period* and *low-exclusion period*, respectively. The three-dimensional images of the positive TFE regions and those of the negative TFE regions are shown in Figure 6. We set all of the Δx, Δy, and Δz in eq 6 to 1.0 Å.

It was understood that the positive TFE regions have planar shapes, and are continuously distributed along the surface of AMb (Figure 6 a and d). In contrast, the negative TFE regions have spherical shapes and are scattered mainly around the side-chains of AMb (Figure 6. b and f). The number and the total volume of the negative TFE regions are larger in the low-exclusion period. On the other hand, occupancy of positive TFE regions on the AMb surface is smaller in this period than that in the high-exclusion period. Throughout the analysis of $\Delta\mathcal{G}_a^{tr}(\mathbf{r})$, the three-dimensional characteristics of TFE, that is, the mixture of the positive and negative TFE regions, were clearly understood.

4. CONCLUDING REMARKS

We performed all-atom MD simulation of AMb in the molecular crowding condition with TMAO. To determine the total amount of TFE and to analyze its spatio−temporal characteristics, we used three types (i.e., radial, surficial, and elemental) of KB integral. Using the radial KB integral, the TFE of AMb from pure water into the aqueous solution of TMAO was calculated from MD-derived radial distribution functions of the solvent components. The time average value of the TFE and the preferential exclusion parameter compared reasonably well with those values obtained from previous experimental studies.

Furthermore, with the aid of the surficial KB integrals, TFE was analyzed as a function of the distance from the AMb surface. Most of the preferential exclusion of TMAO occurred in the vicinity of the AMb surface, and resulted in the positive TFE. The increase and decrease in TFE converged within about 10 Å of the AMb surface. On the other hand, time-resolved KB integrals revealed a large fluctuation in the time history of TFE. The trajectory suggested the possibility that TMAO molecules transiently reduce the preferential exclusion, and stop to act as stabilizers within several nanoseconds. The correlation between, such an alteration in TMAO solvation around AMb and a change in the protein radius of gyration R_g was implied. Finally, the elemental KB integrals provided a detailed three-dimensional picture of the TFE: the mixture of the continuously distributed positive TFE regions and the spherically scattered negative ones.

In accordance with previous experimental measurements, our theoretical approach also reproduced quantitatively the positive TFE value of the protein into the molecular crowding condition with TMAO. In addition to the above time-averaged picture, using the time-resolved KB integrals, it was indicated that the solvation structure of TMAO around the solute, and the TFE of protein in the crowding condition are remarkably dynamic. Furthermore, it was also understood that the spatial distributions of the TFE elements are not homogeneously positive around the protein. These findings provide us with the three-dimensional and the molecular dynamics characteristics of the protein TFE into the molecular crowding condition with TMAO.

APPENDIX

A. Derivative of Solvation Gibbs Energy with Respect to the Number Density of TMAO Molecules

We derive equations for a system with the three components, water, TMAO, and AMb, where AMb is very dilute in the mixture of water and TMAO. The slope of the solvation Gibbs energy of AMb $\Delta\mathcal{G}_a^*$ as a function of the molar fraction of TMAO x_t is obtained as[17,18]

$$\lim_{\rho_a\to 0}\left(\frac{\partial\Delta\mathcal{G}_a^*}{\partial x_t}\right)_{P,T} = \frac{kT(\rho_t+\rho_w)^2}{\eta}(G_{aw}-G_{at}) \tag{A1}$$

where the auxiliary quantity η is as

$$\eta = \rho_w + \rho_t + \rho_w\rho_t(G_{ww}+G_{tt}-2G_{wt}) \tag{A2}$$

The derivative of the $\Delta\mathcal{G}_a^*$ with respect to the number density of TMAO ρ_t is obtained as

$$\lim_{\rho_a\to 0}\left(\frac{\partial\Delta\mathcal{G}_a^*}{\partial\rho_t}\right)_{P,T} = \lim_{\rho_a\to 0}\left(\frac{\partial\Delta\mathcal{G}_a^*}{\partial x_t}\right)_{P,T}\left(\frac{\partial x_t}{\partial\rho_t}\right)_{P,T} \tag{A3}$$

Using the relation

$$\rho_w V_w + \rho_t V_t = 1 \tag{A4}$$

we can rewrite x_t as

$$x_t = \frac{\rho_t}{\rho_t+\rho_w} = \frac{\rho_t}{(1-V_t/V_w)\rho_t + (1/V_w)} \tag{A5}$$

From eqs A4 and A5, we have

$$\begin{aligned}\left(\frac{\partial x_t}{\partial\rho_t}\right)_{P,T} &= \frac{2(1-V_t/V_w)\rho_t + (1/V_w)}{\{(1-V_t/V_w)\rho_t + (1/V_w)\}^2}\\ &= \frac{2V_w(V_w-V_t)\rho_t + V_w}{\{(V_w-V_t)\rho_t + 1\}^2}\\ &= \frac{2(V_w\rho_t + V_w\rho_w) - 1}{V_w(\rho_t+\rho_w)^2}\end{aligned} \tag{A6}$$

From eqs A1, A3, and A6, we get

$$\begin{aligned}&\lim_{\rho_a\to 0}\left(\frac{\partial\Delta\mathcal{G}^*{}_a}{\partial\rho_t}\right)_{P,T}\\ &= \frac{kT(\rho_t+\rho_w)^2}{\eta}\frac{2(V_w\rho_t + V_w\rho_w) - 1}{V_w(\rho_t+\rho_w)^2}(G_{aw}-G_{at})\\ &= kT\frac{2V_w(\rho_t+\rho_w) - 1}{\eta V_w}(G_{aw}-G_{at})\end{aligned} \tag{A7}$$

dx.doi.org/10.1021/jp300380p | J. Phys. Chem. B 2012, 116, 4080−4088

From the relation

$$\eta V_w = 1 + \rho_t(G_{tt} - G_{tw}) \tag{A8}$$

we obtain following relation (eq 8 in the manuscript)

$$\lim_{\rho_a \to 0}\left(\frac{\partial \Delta \mathcal{G}_a^*}{\partial \rho_t}\right)_{P,T} = kT\frac{2V_w(\rho_t + \rho_w) - 1}{1 + \rho_t(G_{tt} - G_{tw})}(G_{aw} - G_{at}) = kT\frac{2V_w(\rho_t + \rho_w) - 1}{\rho_t(G_{tw} - G_{tt}) - 1}(G_{at} - G_{aw}) \tag{A9}$$

B. Atom-Based Kirkwood−Buff Integral

To calculate the three types of KB integrals, $G^R_{\alpha s}(R)$, $G^S_{\alpha s}(R^\upsilon)$, and $G^E_{\alpha s}(\mathbf{r})$, we used the number of the constituent "atoms" of the solvent molecule s. In this case, $N^\phi_{\alpha s}(R,t)$, $N^\upsilon_{\alpha s}(R^\upsilon, t)$, and $N^{\Delta r}_s(\mathbf{r}, t)$ in eqs 3−6 indicate the instantaneous coordination number of the constituent atoms of s inside the integration range $\phi_k(R,t)$, $\upsilon_\alpha(R^\upsilon,t)$, and $\Delta\mathbf{r}$, respectively. Therefore, ρ_s in eqs 3−6 is also substituted by the number density of constituent atoms of s in the bulk solvent phase. This treatment was performed to reinforce the statistical accuracy and to take account of the partial penetration of each solvent molecule into the integration ranges.

■ ASSOCIATED CONTENT

Ⓢ Supporting Information

Three-dimensional distributions of TFE in additional three time durations (t = 12−14 ns, t = 14−16 ns, and t = 16−19 ns) were analyzed and visualized with the same procedure shown in Figure 6. This information is available free of charge via the Internet at http://pubs.acs.org/.

■ AUTHOR INFORMATION

Corresponding Author

*E-mail: yu@chem.aoyama.ac.jp. Tel: +81-42-759-6296. Fax: +81-42-759-6493.

Notes

The authors declare no competing financial interest.

■ ACKNOWLEDGMENTS

This work was supported by Grants-in-Aid for Scientific Research and for Young Scientists (B) (22750015) "Microscopic Breakthrough on the Molecular Crowding Effects Promoting the Function of Biomolecules" from the Ministry of Education, Culture, Sport, Science and Technology in Japan, and for the Core Research for Evolutional Science and Technology (CREST) "High Performance Computing for Multiscale and Multiphysics Phenomena" from the Japan Science and Technology Agency.

■ REFERENCES

(1) Srere, P. A. *Trends Biochem. Sci.* **1981**, *6*, 4−7.
(2) Fulton, A. B. *Cell* **1982**, *30*, 345−347.
(3) Zimmerman, S. B.; Minton, A. P. *Annu. Rev. Biophys. Biomol. Struct.* **1993**, *22*, 27−65.
(4) Miyoshi, D.; Sugimoto, N. *Biochimie* **2008**, *90*, 1040−1051.
(5) Yancy, P. H. *J. Exp. Biol.* **2005**, *208*, 2819−2830.
(6) Kendra, B.; Frederic, D.; Enrique, M. C. *J. Mol. Biol.* **2008**, *378*, 540−550.
(7) Chebotareva, N. A. *Biochemistry (Moscow)* **2007**, *72*, 1478−1490.
(8) Timasheff, S. N. In *Protein−Solvent Interactions*; Gregory, R. B., Eds.; Marcel Dekker: New York, 1995; pp 445−482.
(9) Xie, G.; Timasheff, S. N. *Protein Sci.* **1997**, *6*, 211−221.
(10) Lee, J. C.; Timasheff, S. N *J. Biol. Chem.* **1981**, *256*, 7193−7201.
(11) Gekko, K.; Timasheff, S. N. *Biochemistry* **1981**, *20*, 4667−4676.
(12) Arakawa, T.; Timasheff, S. N. *Biophys. J.* **1985**, *47*, 411−414.
(13) Zou, Q.; Bennion, B. J.; Daggett, V.; Murphy, K. P. *J. Am. Chem. Soc.* **2002**, *124*, 1192−1202.
(14) Yu., I.; Nagaoka, M. *Chem. Phys. Lett.* **2004**, *388*, 316−321.
(15) Yu, I; Jindo, Y.; Nagaoka, M. *J. Phys. Chem. B* **2007**, *111*, 10231−10238.
(16) Kirkwood, J. G.; Buff, F. P. *J. Chem. Phys.* **1951**, *19*, 774−777.
(17) Ben-Naim, A. *Statistical Thermodynamics for Chemist and Biochemist*; Plenum Press: New York, 1992.
(18) Ben-Naim, A. *Molecular Theory of Solutions*; Oxford University Press: New York, 2006.
(19) Yu, I; Takayanagi, M.; Nagaoka, M. *J. Phys. Chem. B* **2009**, *113*, 3543−3547.
(20) Nagaoka, M.; Yu, I; Takayanagi, M. In *Proteins: Energy, Heat and Signal Flow*; Leitner, D. M., Straub, J. E., Eds.; CRC: Boca Raton, FL, 2009; pp 169−196.
(21) Yu, I; Tasaki, T.; Nakada, K.; Nagaoka, M. *J. Phys. Chem. B* **2010**, *114*, 12392−12397.
(22) Greene, R. F.; Pace, C. N. *J. Biol. Chem.* **1974**, *249*, 5388−5393.
(23) Case, D. A.; Darden, T. A.; Cheatham, T. E.; Simmerling, C. L.; Wang, J.; Duke, R. E.; Luo, R.; Crowley, M.; Walker, R. C.; Zhang, W., et al. *AMBER10*; University of California: San Francisco, CA, 2008.
(24) Duan, Y.; Wu, C.; Chowdhury, S.; Lee, M. C.; Xiong, G.; Zhang, W.; Yang, R.; Cieplak, P.; Luo, R.; Lee, T.; et al. *J. Comput. Chem.* **2003**, *24*, 1999−2012.
(25) Fornili, A.; Civera, M.; Sironia, M.; Fornili, S. L. *Phys. Chem. Chem. Phys.* **2003**, *5*, 4905−4910.
(26) Jorgensen, W. L.; Chandrasekhar, J.; Madura, J. D.; Impey, R. W.; Klein, M. L. *J. Chem. Phys.* **1983**, *79*, 926−935.
(27) Berendsen, H. J. C.; Postma, J. P. M; van Gusteren, W. F.; Dinola, A.; Haak, J. R. *J. Chem. Phys.* **1984**, *81*, 3684−3690.
(28) Darden, T.; York, D.; Pedersen, L. *J. Chem. Phys.* **1993**, *98*, 10089−10092.
(29) Ryckaert, J. P.; Ciccotti, G.; Berendsen, H. J. C. *J. Computat. Phys.* **1977**, *23*, 327−341.
(30) Shimiz, S.; Matsubayashi, N. *Chem. Phys. Lett.* **2006**, *420*, 518−522.
(31) Auton, M.; Bolen, D. W.; Rosgen., J. *Proteins* **2008**, *73*, 802−813.
(32) Auton, M.; Bolen, D. W. *Biochemistry* **2004**, *43*, 1329−1342.
(33) Hu, C. Y.; Kokubo, H.; Lynch, G. C.; Bolen, D. W.; Pettitt, B. M. *Protein Sci.* **2010**, *19*, 1011−1022.
(34) Miller, S.; Janin, J.; Lesk, A. M.; Chothia, C. *J. Mol. Biol.* **1987**, *196*, 641−656.